Flow in a weakly curved square duct:
Assessment and extension of Dean's model

Leonardo Rigo, Damien Biau [◉],[*] and Xavier Gloerfelt
Dynfluid Laboratory, École Nationale Superieure d'Arts et Métiers.
and 151 Boulevard de l'Hôpital, 75013 Paris, France

The simplified model by W. R. Dean, based on a low-curvature assumption, provided an early understanding of the laminar flow in curved ducts. However, most of the following studies relied on computer simulations of the complete curvilinear Navier-Stokes equations controlled by two nondimensional parameters, the curvature ratio and the Reynolds number. In the present article an extended version of Dean's model is used and compared to existing results. The set of equations is unsteady, parabolic in a streamwise direction, expressed in Cartesian coordinates, and contains a single control parameter, namely, the Dean number. The equations are identical to those used for the Görtler instability in boundary layer flows. Nonetheless, their extension to duct flows remains to be validated, which is the main purpose of the present article. The model satisfactorily reproduces benchmark results in the literature. In particular we retrieve the successive bifurcations between steady, unsteady, and chaotic regimes for 2D flows. The model also reproduces the development of three-dimensional flow in an elbow with a curvature radius equal to 15.1 times the square duct width. In addition, the present results confirm the Dean number as the single control parameter for laminar flows in a weakly curved ducts.

I. INTRODUCTION

Flows in curved pipes are subject to centrifugal force. At the bend, a centripetal pressure gradient balances the centrifugal force inducing the change in direction to the fluid elements. However, the pressure gradient required by the faster moving elements at the center of the duct is greater than the one required by the slower moving fluid near the walls. This results in the fluid near the centerline moving toward the outside of the pipe and the fluid near the wall moving inwards. Thus, the flow presents two components, a primary flow, parallel to the main direction of fluid motion, and a secondary flow, perpendicular to the primary flow direction. Although the intensity of the secondary flow is a small fraction of the main stream, typically a few percent, it may have important practical implications, having the general role of redistributing friction and heat flux along the duct perimeter.

The curvature effects of tubes on internal flow patterns have been investigated for a long time; nevertheless this issue continues to be an active area of research due to the complexities introduced in specific applications. For overviews on the subject, the reader is referred to Berger *et al.* [1] who present an extensive review on laminar flow in curved pipes, while Kalpakli Vester *et al.* [2] concentrate on the research concerning turbulent and transitional flows while providing a thorough historical review. These two articles refer mainly to circular pipe flows, which are qualitatively very similar to square pipe flows.

---

[*]damien.biau@ensam.eu

Here we present the most relevant contributions to the understanding of the laminar flow in a duct to clarify the current state of the art and the purpose of the present article. Before proceeding, it is useful to introduce the definitions of the characteristic quantities for pipe flows, namely, the fluid density ρ, the bulk velocity U_b, and the dynamic viscosity μ. The geometry is characterized by the duct height h and by the curvature radius R, defined as the distance from the center of curvature to the centerline of the duct. The curvature ratio h/R is thus zero for a straight duct and tends to unity for a duct elbow. The curvature ratio h/R and the Reynolds number $\mathrm{Re} = \rho U_b h/\mu$ are the two control parameters for turbulent flows. However, in laminar flow the Dean number $\mathrm{De} = \mathrm{Re}\sqrt{h/R}$ takes into account both the Reynolds number and the effects of curvature and characterizes the flow for relatively low curvature (see [3]); this nondimensional parameter was first introduced for laminar flow and small curvatures by Dean in 1928 in Ref. [4], p. 678.

The seminal study by Dean [4,5] laid the foundations for the analytical solution of the problem based on a perturbation method. This technique was used in the case of a steady laminar flow in a circular pipe with relatively weak curvature. Dean showed that the only control parameter was $\mathrm{Re}\sqrt{h/R}$ (which he used squared and is nowadays known as the Dean number) and that a cross-flow velocity field consists of two counter-rotating vortex cells where the flow in the center plane was directed toward the outer wall. These counter-rotating vortices are nowadays called Dean cells or Dean vortices. In his first article, Dean [5] took the expansion only to the first order, which was not enough to evaluate the influence of curvature on the pressure drop. In his second paper [4] the expansion was brought to higher order showing a decreasing flow rate with increasing curvature. In a further study Dean and Chapman [6] also considered the curved 2D channel, i.e., unbounded in the spanwise direction. In that case the cross-flow vortices result from an instability of the plane Poiseuille flow, associated to a critical Dean number, in contrast to the pipe geometry where the cells amplitude is proportional to the Dean number. Slightly later, in 1959, Dean and Hurst [7] replaced the actual secondary motion by a uniform wall-normal stream in order to simplify the nonlinear terms and thus the analytical solution. Moreover, with that simplification, results have a more general scope and apply to any form of pipe, circular or square among others. More importantly for the purpose of the present paper, the equations were simplified, replacing the curvilinear coordinates with a Cartesian system.

Dean's series expansion method for the circular duct problem was later brought to higher order by Van Dyke [8] with the use of numerical tools, while McConalogue and Srivastava [9] used an iterative method to solve the early Dean model [4,5]. Apart from the aforementioned studies, most of the following works relied on the rapidly developing computational resources to solve the nonlinear Navier-Stokes equations, also taking advantage of the lateral symmetry of the problem. Some authors concentrated on the rectangular duct geometry (see, e.g., Refs. [10–12]); others studied the circular duct [13,14], finding qualitatively similar results. These studies showed the presence of an additional couple of counter-rotating vortices produced by the Görtler instability on the concave wall, situated at the outer part of the duct. This instability appears for high enough Dean numbers through a subcritical bifurcation [15]; this subcriticality is strongly linked to the arbitrarily imposed lateral symmetry, as later shown by Winters [16]. In particular Cheng *et al.* [12] performed a parametric study for different Dean numbers, showing that for increasing De the flow evolved from two to four circulation cells, returning to a two-cell structure and subsequently back to four cells, hence bearing a nontrivial dependence on De. The two-cell solution is in truth observed only for low De. Daskopoulos and Lenhoff [17] noticed that the two-cell solution presents instead four cells for De close to the critical one, even though the additional cells are rather weak. We will henceforth refer to the two solutions as the weak and strong four-vortices solutions. For a more extensive review on the early numerical and experimental works on the subject, see Refs. [1,18].

Winters [16] largely contributed to the understanding of the Dean problem, specifically referring to the square duct case, clarifying some important aspects. He gave a quantitative criterion for the distinction between low and high curvature, showing that for $h/R > 0.05$ the bifurcation scenario

is governed by two independent parameters, the Reynolds number Re and the geometry h/R, whereas for $h/R < 0.05$ the curvature can be considered as weak and the dynamic is governed by a single control parameter (De). In addition, he shed light on the effect of the symmetry hypothesis, which was found to artificially stabilize the four-vortices solution, thus altering the two- to four-cells bifurcation, which was earlier deemed subcritical [15] but is in fact a supercritical pitchfork bifurcation. Most importantly Winters [16] performed a parametric study by varying the two control parameters; thereby he presented for the first time a bifurcation diagram. Wang and Yang [19] later confirmed these results and expanded the analysis to higher Dean numbers finding periodic oscillations after the symmetry-breaking bifurcation and a chaotic behavior for high De, as also seen in Ref. [20]. In particular the work by Wang and Yang [19] considered a forced convection problem; however, no buoyancy effects are included in the momentum equations, making the results coherent with the present and other studies.

At the same time, other studies focused on the spatial development. The additional complexity with 3D flows comes from the elliptic nature of the equations caused by the incompressibility constraint. Patankar *et al.* [21] presented a calculation procedure for heated flows in helically coiled pipes based on a parabolized version of the Navier-Stokes equations. The axial momentum diffusion and the variation of axial pressure gradient at a cross plane were neglected, allowing a space marching technique. However, this convenient model was introduced without physical justifications. Ravi Sankar *et al.* [22], who followed the method of Patankar *et al.* [21] for flows in curved square ducts, reported periodic structures in the axial direction for Dean numbers above 128. Bara *et al.* [23] presented an experimental and numerical study of the flow development and fully developed flows in a curved square duct with a curvature ratio of 15.1. They reported a steady and symmetric two-vortex flow at De = 125 and a steady and symmetric four-vortex flow at both De = 137 and 150. They introduced asymmetric perturbations at the inflow with a symmetrically positioned pin, confirming the prediction by Winters [16] that four-vortex flows are stable to symmetric perturbations, but unstable to asymmetric perturbations. They also pointed out that the development length of the four-vortex flow decreases with increasing Dean number, which may constitute a limit for the experiments. Mees *et al.* [24] presented new experiments with an inwardly spiraling duct to allow significant development lengths; they were consequently able to confirm the numerical results by Ravi Sankar *et al.* [22] about the steady oscillations in the streamwise direction between two-cell and four-cell states for Dean numbers between 139 and 240. With the same numerical method and experimental apparatus, Mees *et al.* [25] observed the development of a six-cell secondary flow pattern above a Dean number of 350. In those articles [23–25], the measured velocity profiles and flow visualizations are in good agreement with the simulations, confirming that the parabolized Navier-Stokes equations give an accurate description of the entry flow. Nonetheless, the limits of the model are unknown in the lack of physical assumptions underlying the parabolic approximation.

From this bibliographical survey it appears interesting to consider a simpler model, able to reproduce the main characteristics of the flow in a weakly curved square duct. One may wonder if a basic model, related to the idea evoked by Dean and Hurst [7], would be capable of accurately representing the flow features in terms of dynamics and bifurcations, and up to what limit of curvature. Such analysis, in addition to providing and validating a very simple tool for the calculation of the flow in a bent duct, would clarify whether the terms neglected in the simplification do or do not play a relevant role for the flow under scrutiny.

In the following we applied the parabolic equations, first introduced by Floryan and Saric [26] and Hall [27] in the context of the boundary layer flows, to the weakly curved square duct. That model will be exposed in the next section, followed by validations of the results for the successive bifurcations of 2D flows and 3D entry flows. In conclusion, the salient features of the present model are exposed followed by a discussion about the possible extension to turbulent flows. In the Appendix some quantitative results are provided for validation purposes, as well as discussion of the Python code used for the numerical solution [46].
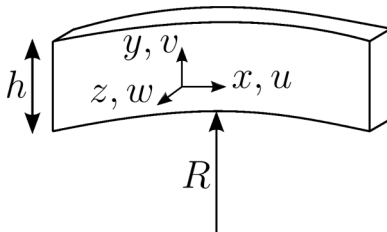
FIG. 1. Representation of the Cartesian coordinates system in a weakly curved duct.

II. METHOD

Before introducing the low-curvature assumption, we start with curvilinear framework, where r, x, θ are the radial, axial, and azimuthal coordinates, respectively, and R is the centerline curvature radius. In this paper we will focus on the laminar flow in a square duct; however, the model can be applied to ducts of arbitrary cross section. Assuming relatively low curvature, namely, $h/R \ll 1$ with h being the duct height, the global polar coordinates can be approximated by the local Cartesian coordinates shown in Fig. 1. In the following $(x, u), (y, v), (z, w)$ denote the local Cartesian system in the streamwise, radial, and cross stream directions and velocities, respectively, with

$$y := r + R \approx R \quad \text{and} \quad x := R\theta.$$

The principal parameters for a duct flow are the duct height h, the kinematic viscosity ν, and the bulk velocity:

$$U_b := \frac{1}{S} \int_S u \, dy \, dz, \tag{1}$$

so the Reynolds number is defined as

$$\text{Re} = \frac{U_b h}{\nu}. \tag{2}$$

We use the following nondimensional quantities (the asterisk indicates the dimensional variables):

$$u = \frac{u^*}{U_b}, \quad v, w = \frac{v^*, w^*}{\nu/h}, \quad p = \frac{p^*}{\rho(\nu/h)^2},$$

$$x = \frac{x^*}{h \, \text{Re}}, \quad y, z = \frac{y^*, z^*}{h}, \quad t = \frac{t^*}{h^2/\nu}. \tag{3}$$

By injecting these scaling laws in the equations and neglecting the terms of $O(\text{Re}^{-2})$, $O(h/R)$, and higher, we obtain

$$\frac{\partial u}{\partial x} + \frac{\partial v}{\partial y} + \frac{\partial w}{\partial z} = 0, \tag{4a}$$

$$\frac{\partial u}{\partial t} + u\frac{\partial u}{\partial x} + v\frac{\partial u}{\partial y} + w\frac{\partial u}{\partial z} = -\frac{d\tilde{P}}{dx} + \frac{\partial^2 u}{\partial y^2} + \frac{\partial^2 u}{\partial z^2}, \tag{4b}$$

$$\frac{\partial v}{\partial t} + u\frac{\partial v}{\partial x} + v\frac{\partial v}{\partial y} + w\frac{\partial v}{\partial z} - De^2 u^2 = -\frac{\partial p}{\partial y} + \frac{\partial^2 v}{\partial y^2} + \frac{\partial^2 v}{\partial z^2}, \tag{4c}$$

$$\frac{\partial w}{\partial t} + u\frac{\partial w}{\partial x} + v\frac{\partial w}{\partial y} + w\frac{\partial w}{\partial z} = -\frac{\partial p}{\partial z} + \frac{\partial^2 w}{\partial y^2} + \frac{\partial^2 w}{\partial z^2}. \tag{4d}$$

The Dean number is defined as

$$\mathrm{De} = \mathrm{Re}\sqrt{\frac{h}{R}}. \tag{5}$$

Those equations have been introduced in the context of the Görtler instability in linear [26,27] and nonlinear [28] frameworks. For an overview on the subject, the reader is referred to Saric [29]. The curvature effect is reduced to a single term in a Cartesian framework: the nondimensional centripetal acceleration $-\mathrm{De}^2 \cdot u^2$.

The main pressure gradient, $d\tilde{P}/dx$, that drives the duct flow does not depend on cross-flow coordinates; it is adjusted dynamically to maintain a constant mass flux, and it must be distinguished from the cross-flow gradient of the hydrodynamic pressure p present in the other equations.

The streamwise pressure gradient and diffusion terms are neglected, hence the equations are parabolic in x, allowing a space marching technique. As a consequence, the present model requires that the streamwise velocity component is positive everywhere, which excludes streamwise flow separation, which may happen for strong curvatures. The streamwise parabolic equations offer a simple and fast approach for the modeling of spatially developing flows, and their simplicity and low computational cost make them a powerful complement to rigorous elliptic and curvilinear problems.

Slightly different versions of the parabolized equations have appeared in the literature. These versions differ in the presence or not of a streamwise pressure gradient term. However, in all cases the second derivative terms with respect to the streamwise direction is omitted. Davis and Rubin [30] call the set of equations not containing a streamwise pressure gradient term the parabolic Navier-Stokes equations, and the sets of equations that do contain a streamwise pressure gradient term the parabolized Navier-Stokes equations. The numerical solutions provided in Refs. [21–23,31] among others rely on a parabolized model, obtained without a formal justification.

Equations (4) are solved with Chebyshev collocation method in inhomogeneous directions (y, z) in conjunction with no-slip boundary condition at the walls. The divergence-free condition is achieved with the prediction-projection scheme by Chorin and Temam (for an exhaustive review of projection methods see Ref. [32]). Pressure is computed using polynomials of two orders less than those used for the velocities, in order for the pressure field to remain unpolluted of spurious modes. Hence, the same grid is used for pressure and velocity fields, and no pressure boundary conditions are required. For further details on the accuracy and stability of the method see Ref. [33]. This numerical method was found to be accurate enough to compute the subcritical transition to turbulence in square duct flows [34].

For the 2D flows, i.e., invariant in the streamwise direction (x), the temporal discretization is realiszd with a fourth-order time marching scheme, with the viscous term treated implicitly [35]. The results have been obtained with a grid composed of $Ny \times Nz = 31 \times 31$ Chebyshev points, with a time step (Δt) of 1.2×10^{-5}. Details of the Python program for the solution of the 2D problem are provided in the Appendix.

The 3D solutions are obtained by means of a MacCormack prediction-correction algorithm [36]. We impose a velocity profile at the inlet, for example, the straight laminar flow solution. No boundary condition is required at the outflow due to the convective nature of the equations. The simulations are performed considering a domain of length 20/De on a grid composed of 31 Chebyshev points in both wall normal directions and 200 equispaced points in the streamwise direction. The time step is $\Delta t = 10^{-4}$ nondimensional time units. It should be mentioned that for the 3D parabolic equations, despite the prediction-projection scheme by Chorin-Temam, the divergence does not reach machine precision but remains within reasonable limits. The infinity norm of the velocity divergence is of order 10^{-4} with a $200 \times 31 \times 31$ grid, and of order 10^{-8} with a $200 \times 101 \times 101$ grid, without significant change for the presented results. The same issue was encountered by Ravi Sankar *et al.* [22], who report a divergence of order 10^{-4}, indicating that that issue seems to be related to the nature of the equations applied to duct flows.

In the next section, the model is confronted against benchmark results. It should be noted that the Dean number takes various forms in the literature, sometimes based on the constant pressure

gradient in analytical or numerical studies, sometimes on the centerline velocity in stability analyses, and sometimes on the mean velocity in the pipe, mostly in experimental studies. Those differences are a source of confusion in the interpretation of the results from the literature as discussed in Ref. [1]. In the present article, when referring to papers where the authors have used a different definition of the Reynolds and/or Dean numbers, we recalculate them to adhere to the present definition. Specifically, we will compare our results mostly with those reported by Wang and Yang [19], who use the pressure gradient definition of the Dean number that they call the pseudo-Dean number D_k. The same authors provide a conversion table between D_k and De, as defined here (see Table 3 of Ref. [19]). When not directly available in the table the values of De are obtained by interpolation on the quasilinear dependency curve between De and D_k.

III. RESULTS

The extended Dean's model presented above is mathematically appealing since the equations are expressed in Cartesian coordinates and are parabolic in the streamwise direction. Curvature effects are retained through a single term coupling the streamwise velocity to the cross-flow vortices; moreover the Reynolds number and curvature ratio are combined to form a single governing parameter, the Dean number. Nonetheless, the inherent approximations need to be validated against existing results. In this section we consider the successive bifurcations of 2D flow (i.e., homogeneous in the streamwise direction), and the periodic solution is also analyzed through linear stability results. We eventually investigate the development of an initially straight flow entering a curved section.

A. Two-dimensional flow: The bifurcation diagram

In two dimensions the solutions can be distinguished according to their symmetry in the wall normal direction (z):

Symmetric solutions:

$$u(0.5 + z) = u(0.5 - z),$$
$$v(0.5 + z) = v(0.5 - z),$$
$$w(0.5 + z) = -w(0.5 - z),$$

Antisymmetric solutions:

$$u(0.5 + z) = -u(0.5 - z),$$
$$v(0.5 + z) = -v(0.5 - z),$$
$$w(0.5 + z) = w(0.5 - z).$$

In order to determine whether the system is stationary, periodic, aperiodic, or chaotic we use a Poincaré-like section based on the following three criteria:

$$v = 0, \quad \frac{\partial v}{\partial t} < 0, \quad \text{and} \quad w < 0,$$

measured in a specific point located at the centerline close to the outer wall, specifically at $y = 0.9045$, $z = 0.5$. These conditions are met only once per period, thus if the oscillation is periodic the system will cross the section every T time units, and the numerical values will be the same.

Figure 2 shows the squared velocity 2-norm defined as

$$||\boldsymbol{u}||_2^2 = \frac{1}{2} \int_S u^2 + \frac{v^2 + w^2}{\text{De}^2} \, dS,$$

as a function of the Dean number. The open circles correspond to the stationary regimes. At very low De we observe the symmetric two vortices solution: a first change in behavior is observed at De = 124 with the formation of a second pair of vortices at the external wall, very weak in intensity.
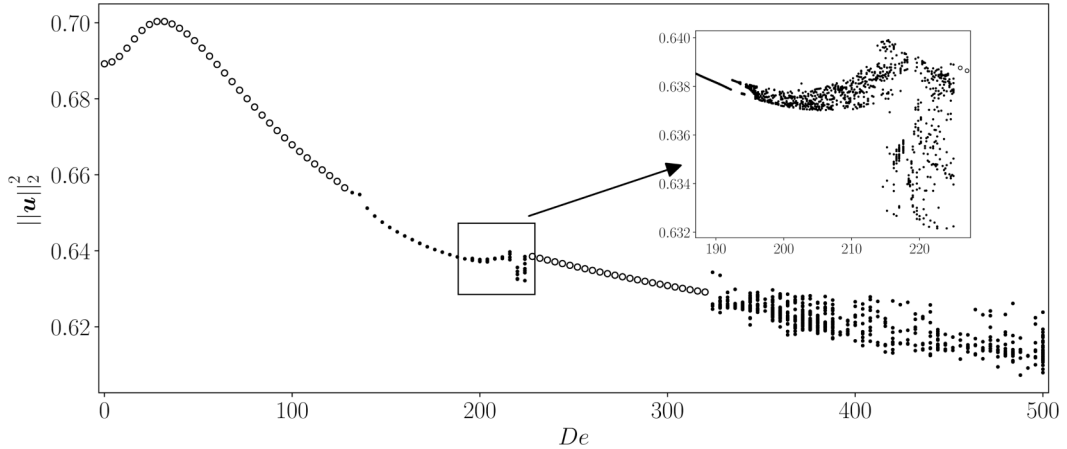
FIG. 2. Filled circles: values of the squared 2-norm of the velocity vector at the instants when the Poincaré section is crossed. Open circles: values of the square of the 2-norm of the velocity vector in the stationary cases. The first bifurcation from a steady regime to an unsteady, periodic regime occurs at De = 128.32. Starting from De ≈ 193 we observe two periods which are incommensurable, characteristic of an aperiodic regime. Then the system quickly evolves into chaos from De ≈ 195. For De ∈ [227, 318] the system is again stationary, and after a narrow periodicity interval the system becomes again chaotic at De = 324. A magnification of the bifurcation diagram for De ∈ [190, 230] is shown in the inset

We thus have the formation of the weak four-vortices solution, the change in behavior occurs on the same branch, and no bifurcations are observed in agreement with Watanabe and Yanase [37]. The first bifurcation from a steady regime to an unsteady, periodic regime occurs at De = 128.32. This specific Dean number will henceforth be referred to as the critical Dean number De_c. In Fig. 2 the black dots represent the values of the squared 2-norm of the velocity vector at each crossing of the Poincaré-like section, for each De the simulation was run for at least 10 periods, hence the periodic behavior is represented in Fig. 2 by at least 10 superposed points.

The system holds its periodicity until De ≈ 193, where it becomes aperiodic. Wang and Yang [19,38] also observed a change in behavior in that Dean number range, namely, a slight increase and then a decrease in the period, but they did not mention observing aperiodicity. The aperiodic regime is observed only over a narrow range of De; already at De = 195 the system is complex enough to be considered chaotic. Analyzing the magnified part in Fig. 2, we notice the presence of a new solution branch to which the system abruptly jumps back and forth. The increase in complexity is then very rapid; between De = 125 and 214 the system is chaotic with values of the velocity norm that remain enclosed in the envelope of the two former branches.

Between De = 214 and 227 the values no longer lie within the same envelope, probably due to the presence of a third branch (which was indeed observed by Wang and Yang [19]). For De > 227 the system very quickly returns to a stationary regime, which lasts until De = 318, where very mild, periodic oscillations are observed up to De = 323. For higher Dean numbers the system rapidly becomes again chaotic, no stationary or periodic regimes were observed beyond the Dean numbers reported in Fig. 2.

The changes in regime observed for the present model are in very good agreement with the literature. In particular the critical Dean number given by the model, $De_c = 128.32$, is in excellent accordance with the $De_c = 128.22$ by Wang and Yang [19], which is the most accurate study available, or $De_c = 129.71$ by Winters [16]. Both these results were obtained by solving the full 2D Navier-Stokes equations in polar coordinates without low-curvature approximation, thus with two control parameters.
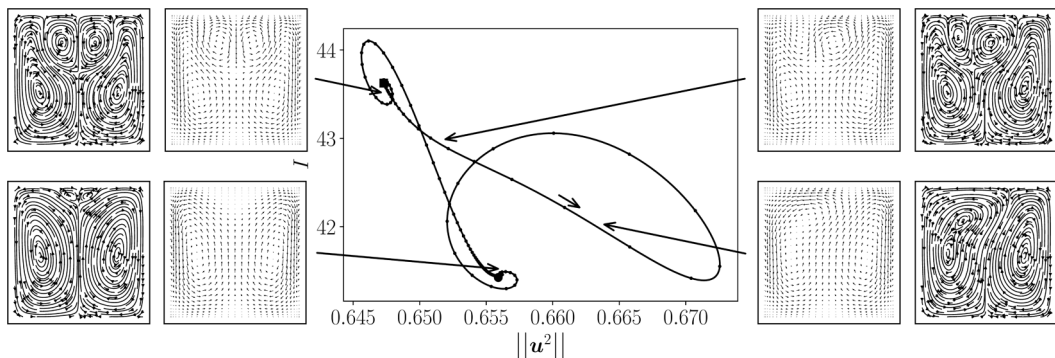
FIG. 3. Injection-velocity norm phase diagram at De = 130. The system follows a periodic orbit passing close to the two stationary solutions, indicated by the solid circle ($I \approx 41.5$, $||\boldsymbol{u}||_2^2 \approx 0.655$) and the solid square ($I \approx 43.5$, $||\boldsymbol{u}||_2^2 \approx 0.647$). The small dots along the curve are recorded for a constant Δt. The higher density of points near the the two stationary solutions indicates the attractive nature of these fixed points. The long arrows indicate the instantaneous states of the system. The flow evolves following the small arrow: from the weak four-cells, symmetric state to the symmetric strong four-cells, when symmetry is broken a kinetic energy burst is observed. The system then returns to a weak four-cells state regaining its symmetry.

The bifurcation to a new steady state occurs at De = 227 with our model, which is slightly above the value obtained in Ref. [19], De = 217. The agreement is better for the next bifurcation to chaos, which is at De = 323 for both models. Nonetheless a difference is observed at the end of the stationary region: in the section between De = 318 and 323 our model produces slight periodic oscillations, while Ref. [19] reports an aperiodic oscillation from De = 312 until the beginning of the chaotic region at De = 323.

B. Two-dimensional flow: The periodic regime

In the interval $128.32 < \mathrm{De} < 193$ the trajectory approaches and leaves periodically the vicinity of two equilibrium states, where the fluid's dynamics slows down and its velocity fields resembles that of the equilibrium. These two equilibria are symmetric with respect to the wall normal direction (z) and are sometimes referred to as the two- and four-vortices solutions [10,11,14,16]. As discussed in the introduction, the oscillations occur between the the strong and the weak four-vortices solutions, as also observed in Refs. [17,19,37]. The vector fields of these two solutions are shown on the left part of Fig. 3. In order to better assess the validity of the model we compared the oscillation period with the one provided in Ref. [19]; at De = 182.2 they report $T = 0.159$, and the present model gives $T = 0.1579$ at the same De.

Both the weak and strong four-vortices steady solutions are observed even for subcritical Dean numbers. The strong four-vortices solution is linearly unstable to nonsymmetric perturbations (and stable otherwise) [16,23], whereas for De $<$ De$_c$ the weak four-vortices solution is linearly stable. This behavior is retrieved by the model and can be shown by performing a linear stability analysis of those two equilibrium states at De$_c$. The Navier-Stokes equations are linearized around either of the steady-state solutions, and the perturbations are expressed in the form

$$q(y, z, t) = \sum_n Q_n(y, z) e^{\sigma_n t} \tag{6}$$

where Q_n is the nth eigenmode associated to the eigenvalue σ_n. The real and imaginary parts of σ are the growth rate and the pulsation, respectively. The equilibrium state is unstable if the real part of at least one σ_n is positive and stable otherwise. The asymptotic behavior is determined by the

TABLE I. Growth rate of the least stable eigenmode of the strong and weak four-vortices solutions at $De_c = 128.32$, obtained with the linear stability analysis. The convergence was stopped when the change in value dropped below 10^{-4}. The eigenvalues can be considered as real; the pulsation is below the threshold 10^{-4}.

	Symmetry	Antisymmetry
Strong four vortices	-40.20	$+44.215$
Weak four vortices	-0.540	-22.371

least stable mode. Numerically this least stable mode is calculated with

$$\sigma = \frac{1}{\int_S q^* q \, dS} \int_S q^* \frac{\partial q}{\partial t} \, dS \tag{7}$$

(the asterisk denotes the complex conjugate) until convergence in the growth rate. The linear simulations are performed by imposing symmetry or antisymmetry. Table I shows the eigenvalues of the most amplified mode for the weak and strong four-vortices solutions and for symmetric and antisymmetric perturbations. Similar to results in the literature previously mentioned, the strong four-vortices solution is stable to symmetric perturbations and unstable to antisymmetric ones. The weak four-vortices solution is linearly stable to any perturbations in the subcritical regime, and the symmetric mode becomes unstable for $De > De_c = 128.32$.

Thus, when the system is perturbed for $De < De_c$, it evolves close to the strong four-vortices solution, which is a saddle point; the trajectory is then ejected, and the system eventually reaches the weak four-cell solution, which is the global attractor. This is the reason why the latter is the observed solution in direct numerical simulations or experiments in the subcritical regime. For $De > De_c$, the weak four-vortices solution becomes linearly unstable, and a perturbation will therefore initiate a cycle between these two solutions. The periodic orbit of the system at $De = 130$ is depicted in Fig. 3 in a state space diagram spanned with the energy injection $I = -d\tilde{P}/dx \, U_b$ and squared velocity 2-norm.

The system follows the direction indicated by the small arrow in the center of Fig. 3. Starting in the proximity of the weak four-vortices solution (indicated with the circle at the bottom left) the flow evolves towards the strong four-vortices solution (indicated with the square at the top left). The system then loses its symmetry, which is consistent with the antisymmetric unstable mode of this solution indicated in Table I. The two upper vortices collapse into one lateral vortex, producing a burst. The system then rapidly returns to a symmetric state, namely, the weak four-vortices solution.

In other words, the trajectory is attracted by the symmetric stable manifold of the strong four-vortices equilibrium; it then leaves this saddle point along the asymmetric manifold toward the weak four-vortices equilibrium. If $De > De_c$, then the weak four-vortices equilibrium becomes unstable to symmetric perturbations (see Table I), and the trajectory is ejected along a second heteroclinic orbit, toward the strong four-vortices equilibrium state, closing the cycle. These two heteroclinic orbits between the two equilibria constitute a heteroclinic cycle which can be suppressed by imposing spanwise symmetry. The mechanism by which that heteroclinic cycle appears is related to a saddle-node bifurcation, [39]. Slightly above the critical Dean number De_c, the period of the limit cycle behaves like $(De - De_c)^{-0.53}$. That heteroclinic cycle was also observed in Ref. [37] for 3D solutions, with streamwise periodic boundary condition.

As a final remark, it is worth mentioning that 2D simulations are unlikely be representative of real unsteady flows. Some authors [20,38,40] assert that periodic regime implies the presence of traveling waves, which were indeed experimentally observed by Mees *et al.* [24,41]. In any case, the 2D curved square duct problem is *per se* an intriguing dynamical system, with several bifurcations depending on one control parameters. We include in the Appendix discussion of a Python program able to reproduce the previous results in two dimensions [46].
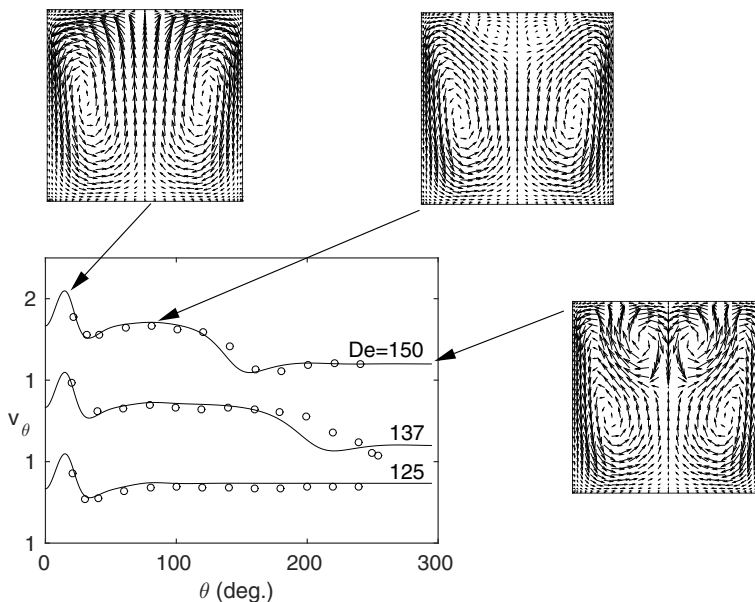
FIG. 4. Streamwise velocity at $y = 0.74$, $z = 0.5$ for De = 125, 127, 150, 3D flow development problem with straight, laminar inflow. Computed with the present parabolic model (lines), compared with the experiments by Bara *et al.* [23] (circles). Cross-flow velocity vectors are shown at $\theta = 12°$, $80°$, and $300°$.

IV. THREE-DIMENSIONAL FLOW: ENTRY FLOW DEVELOPMENT

A practical application for the present model concerns the flow development problem, namely, a straight, laminar flow entering in a curved section. Since curved tubes in engineering applications are often too short for flows to reach the fully developed state, the formulation of transport mechanisms should portray developing conditions. Equations (4) are solved with the straight laminar flow solution at the inlet. The simulations are realized with a domain of length 20/De.

Figure 4 shows the variation of the streamwise velocity u along the streamwise direction at $y = 0.74$, $z = 0.5$, hence towards the middle of the top half of the domain in the radial direction y and in the center in the spanwise direction z.

We use the same display as Fig. 6 in Bara *et al.* [23]. The circles represent the experimental results [23]. The azimuth is obtained from the nondimensional streamwise coordinate x through the relation $\theta = x \sqrt{h/R}\,\text{De}\,180/\pi$, with the ratio $R/h = 15.1$ employed in Ref. [23]. As a consequence of the divergence-free condition, the characteristic streamwise length L must satisfy the following orders of magnitude: $h \ll L = O(\text{Re} = \text{De}\sqrt{R/h})$. Hence, the model is unable to capture small-scale behavior in the streamwise direction. In the case presented in Fig. 4, the cutoff is $\theta = 3.8°$. Despite those limitations, the agreement with the experiment is satisfactory, especially since the inlet velocity profiles in the experiment by Bara *et al.* [23] were not exactly the established straight duct solution.

The spatial oscillations observed of the streamwise velocity can be explained in the same way as the temporal periodic solution described in the previous section. Initially the symmetric two Dean's vortices emerge, then the weak four-vortices solution develops, followed by the formation of the strong four vortices, which are characterized by a lower streamwise velocity in the point examined in Fig. 4 compared to the weak four-vortices solution. These streamwise vortices are the result of two different physical mechanisms. First, for a confined curved flow, like in duct or pipe, the centripetal acceleration $(-\text{De}^2 \cdot u^2)$ is in equilibrium with the radial pressure gradient $(\partial p/\partial y)$. Thus pressure is nonhomogeneous in a spanwise direction, and as a consequence there is

a spanwise pressure gradient ($\partial p/\partial z \neq 0$) which induces spanwise flow ($w \neq 0$). This mechanism is responsible of the so-called Dean vortices [4,5,7], which correspond to the two-vortices steady solution mentioned above. Second, for a flow over a concave wall, when the wall-normal pressure gradient ($\partial p/\partial y$) is strong enough, it can give rise to streamwise counter-rotating vortices; this phenomenon is known as the Taylor-Görtler instability. The spanwise wavelength increases with the Dean number. The concomitance of these two mechanisms leads to the complexity mentioned above, with the observation of four strong or weak cells [37], and the possibility to observe six or more cells for higher Dean number; see Ref. [25].

The good agreement between the models and the experiment demonstrates that the Dean model is capable of capturing all of the laminar flow features, eliminating the complexity of solving the cylindrical Navier-Stokes equations by allowing the use of a Cartesian solver. As well as the model in Ref. [22] the present model can be used for spirals or S-like geometries just by providing the desired law of dependence De(x). Moreover it is time dependent, and as such it can be readily employed to solve problems with moving or elastic walls (Dean number varying with x and time) or with time-dependent inflow conditions. With little modification, i.e., the addition of the curvature term in the z direction, it can be adapted to account for twisted geometries similar to the one studied by Castelain *et al.* [42].

In addition to the validation cases presented so far, the model is also able to reproduce steady and traveling wave solutions observed in the literature for the Dean flow. Mees *et al.* [41] experimentally observed fully developed traveling wave solutions for Dean numbers between 170 and 260, resulting from a secondary shear instability of the spanwise inflectional profile created by the Dean vortices. This convective secondary instability was induced by a pin positioned close to the inlet. Watanabe and Yanase [37] also obtained traveling wave solutions by imposing periodic boundary conditions in the axial direction. A preliminary analysis performed with the present model also showed the traveling wave solution when periodic boundary condition are imposed in the streamwise direction.

V. CONCLUSION AND PERSPECTIVES

In this article, we validate the streamwise parabolic Navier-Stokes equations to describe flows in weakly curved ducts. The equations are expressed in a Cartesian coordinate system, and involve a single control parameter, the Dean number De $= \sqrt{h/R}\,$Re, which comprehends curvature, inertia, and viscous effects. Hence, both numerical and physical complexities are reduced. The model is based on large curvature ratio $h/R \ll 1$ and large Reynolds number assumptions.

In order to assess the applicability domain, comparisons were made against existing, well-established results. For 2D dimensional flows, the successive bifurcations from steady to chaotic regimes are found. Notably, for the unsteady bifurcation, the present model predicts a critical Dean number $\text{De}_c = 128.32$ very close to the value $\text{De}_c = 128.22$ obtained by Wang and Yang [19] with complete Navier-Stokes equations.

For the 3D case, the experiments by Bara *et al.* [23] were realized with $h/R = 1/15.1 = 0.066$. For the 2D simulations, Wang and Yang [19] and Winters [16] used $h/R = 0.02$. We can thus be confident that the model's predictions are reliable at least up to a curvature $h/R = 0.02$ and most probably up to $h/R = 0.066$. Below that limit, it can thus be stated that the Dean number alone characterizes flow similarity in differently bent square ducts, in agreement with Cieślicki and Piechna [3]. The present analysis also confirms the relevance of parabolic hypothesis employed previously; see Refs. [22,23,41] among others.

The model can directly be used to investigate pulsatile flows, or variable curvature geometries such as serpentines or spirals. The application to heat and mass transfers in curved pipes is also straightforward with the addition of the heat equation; see Ref. [21]. Practical configurations could then be investigated such as the heating and cooling coils used in heat exchangers and refrigeration equipment. For example, the onset of a chaotic regime shown in the previous section can have beneficial effects on transfer properties of the flow; indeed, Fellouah *et al.* [43] showed that in the chaotic regime the temperature distribution is more uniform as compared to the Dean vortices case,

TABLE II. Comparison between two calculations at De = 150; the quantities reported are averaged over one time period. The coarser space (N, number of grid points) and time discretizations (third line of the table) are those used in the rest of the paper; the finer simulation is used as a benchmark. Very few differences are observed in the results: the period T varies by a quantity compatible with the Δt itself; the average pressure gradient dP/dx and the streamwise and spanwise dissipations ε_u, ε_{vw} exhibit very limited differences. The differences between the streamwise pressure gradient (equal to the energy injection since $U_b = 1$) and the streamwise dissipation indicate the level of convergence of the respective calculations.

$N_y \times N_z$	Δt	T	dP/dx	ε_u	$\varepsilon_{vw}/\mathrm{De}^2$
101×101	1×10^{-6}	0.20132	−44.5091	44.5066	11.43055
31×31	1.2×10^{-5}	0.2013	−44.513	44.5130	11.43557

in which they observed the formation of overheating zones that are not efficiently mixed by the Dean vortices. Also, Reynolds averaged Navier-Stokes simulations are possible by supplementing a turbulent model [31].

The future developments of the present work concern the study of the effects of curvature on turbulence; see the recent review by Kalpakli Vester *et al.* [2]. Notably, the laminar to turbulent transition has been shown to be deeply affected by curvature switching from subcritical to supercritical when the pipe is sufficiently curved [44,45]. Nonetheless, in order to investigate turbulent flows, the present model is limited by the cutoff of streamwise length scales, $L = O(\sqrt{hR}) \gg h$. To overcome that constrain, a multiple-scale analysis will be necessary. Such a new model could fill the gap in the low-curvature limit, which is numerically challenging when using the complete curvilinear Navier-Stokes equations.

APPENDIX: THE NUMERICAL SCHEME FOR THE 2D CALCULATIONS

The source of the Python program used to generate the data shown in this paper is available in the Supplemental Material [46]. This version of the code mostly contains the calculating core of the program, while most of the postprocessing part was not included for clarity. Some quantities of interest are however added for validation purposes (the streamwise pressure gradient and the dissipation in streamwise x and cross-flow directions y, z). The reader is encouraged to run the program and compare the results obtained with those reported in Table II.

The error in the oscillation period is of the same order of the time step, the differences in the streamwise pressure gradient and streamwise and cross-stream dissipations averaged on one time period are below 5%, despite a more than 10-fold increase in the number of grid points and a 12 times finer time step. The agreement between the average dissipation and pressure gradient in the streamwise direction testifies to the convergence of the calculations.

The simulation is initialized with the laminar solution plus a random velocity field; thus the initial transient exhibits little differences from run to run. The "functions" file is composed of four methods, inserted in a class for practicality. The "constBulk" method uses a bisection algorithm to iteratively calculate the streamwise pressure gradient required to maintain the target streamwise bulk velocity ($U_b = 1$ in the present paper). The "Chebyshev" method is used to define the grid, the derivation matrices for velocity and pressure, and the integration weights. The other two methods are auxiliaries for the "Chebyshev" method. The first part of the "main" file serves as initialization; here we define the operators for derivations and integrations in y and z, the extrapolation (c_i, d_i), and the time integration (a_1, b_i) coefficients. Finally we set the initial condition with the laminar flow solution in a straight duct ($Ulam$), with some additional random noise.

The following part is the actual time loop. In the first part we compute the right-hand-side term (explicit) of the equations, then the solution is updated for the next time steps before calculating the new predicted velocity field. This is then corrected to enforce the divergence-free condition following the prediction-projection method by Chorin and Temam. As a last step of the loop the

streamwise pressure gradient is calculated using the bisection method mentioned above, and the streamwise velocity is corrected as well. The present results were obtained by running the program on a Linux machine using the Anaconda distribution of Python version 3.6.4. The code also works on Python 2.7 (a test was run on the Anaconda distribution of Python 2.7.16).

---

[1] S. A. Berger, L. Talbot, and L. S. Yao, Flow in curved pipes, Annu. Rev. Fluid Mech. **15**, 461 (1983).

[2] A. Kalpakli Vester, R. Örlü, and P. H. Alfredsson, Turbulent flows in curved pipes: Recent advances in experiments and simulations, Appl. Mech. Rev. **68**, 050802 (2016).

[3] K. Cieślicki and A. Piechna, Can the Dean number alone characterize flow similarity in differently bent tubes? J. Fluids Eng. **134** (2012).

[4] W. R. Dean, LXXII. The stream-line motion of fluid in a curved pipe (second paper), London Edinburgh Dublin Philos. Mag. J. Sci. **5**, 673 (1928).

[5] W. R. Dean, XVI. Note on the motion of fluid in a curved pipe, London Edinburgh Dublin Philos. Mag. J. Sci. **4**, 208 (1927).

[6] W. R. Dean and S. Chapman, Fluid motion in a curved channel, Proc. R. Soc. London A **121**, 402 (1928).

[7] W. R. Dean and J. M. Hurst, Note on the motion of fluid in a curved pipe, Mathematika **6**, 77 (1959).

[8] M. Van Dyke, Extended Stokes series: Laminar flow through a loosely coiled pipe, J. Fluid Mech. **86**, 129 (1978).

[9] D. J. McConalogue and R. S. Srivastava, Motion of a fluid in a curved tube, Proc. R. Soc. London A **307**, 37 (1968).

[10] K. C. Cheng and M. Akiyama, Laminar forced convection heat transfer in curved rectangular channels, Int. J. Heat Mass Transf. **13**, 471 (1970).

[11] B. Joseph, E. P. Smith, and R. J. Adler, Numerical treatment of laminar flow in helically coiled tubes of square cross section. Part I. Stationary helically coiled tubes, AIChE J. **21**, 965 (1975).

[12] K. C. Cheng, R. C. Lin, and J. W. Ou, Fully developed laminar flow in curved rectangular channels, J. Fluids Eng. Trans. ASME **98**, 41 (1976).

[13] S. C. R. Dennis and M. Ng, Dual solutions for steady laminar flow through a curved tube, Q. J. Mech. Appl. Math. **35**, 305 (1982).

[14] S. Yanase, N. Goto, and K. Yamamoto, Dual solutions of the flow through a curved tube, Fluid Dynamics Res. **5**, 191 (1989).

[15] R. Shanthini and K. Nandakumar, Bifurcation phenomena of generalized Newtonian fluids in curved rectangular ducts, J. Non-Newtonian Fluid Mech. **22**, 35 (1986).

[16] K. H. Winters, A bifurcation study of laminar flow in a curved tube of rectangular cross-section, J. Fluid Mech. **180**, 343 (1987).

[17] P. Daskopoulos and A. M. Lenhoff, Flow in curved ducts: Bifurcation structure for stationary ducts, J. Fluid Mech. **203**, 125 (1989).

[18] H. Itō, Laminar flow in curved pipes, ZAMM-J. Appl. Math. Mech./Z. Angew. Math. Mech. **49**, 653 (1969).

[19] L. Wang and T. Yang, Bifurcation and stability of forced convection in curved ducts of square cross-section, Int. J. Heat Mass Transf. **47**, 2971 (2004).

[20] R. N. Mondal, Y. Kaga, T. Hyakutake, and S. Yanase, Bifurcation diagram for two-dimensional steady flow and unsteady solutions in a curved square duct, Fluid Dynamics Res. **39**, 413 (2007).

[21] S. V. Patankar, V. S. Pratap, and D. B. Spalding, Prediction of laminar flow and heat transfer in helically coiled pipes, J. Fluid Mech. **62**, 539 (1974).

[22] R. S. Ravi Sankar, K. Nandakumar, and J. H. Masliyah, Oscillatory flows in coiled square ducts, Phys. Fluids **31**, 1348 (1988).

[23] B. Bara, K. Nandakumar, and J. H. Masliyah, An experimental and numerical study of the Dean problem: Flow development towards two-dimensional multiple solutions, J. Fluid Mech. **244**, 339 (1992).

[24] P. A. J. Mees, K. Nandakumar, and J. H. Masliyah, Steady spatial oscillations in a curved duct of square cross-section, Phys. Fluids **8**, 3264 (1996).

[25] P. A. J. Mees, K. Nandakumar, and J. H. Masliyah, Instability and transitions of flow in a curved square duct: The development of two pairs of Dean vortices, J. Fluid Mech. **314**, 227 (1996).

[26] J. M. Floryan and W. S. Saric, Stability of Görtler vortices in boundary layers, AIAA J. **20**, 316 (1982).

[27] P. Hall, The linear development of Görtler vortices in growing boundary layers, J. Fluid Mech. **130**, 41 (1983).

[28] P. Hall, The nonlinear development of Görtler vortices in growing boundary layers, J. Fluid Mech. **193**, 243 (1988).

[29] W. S. Saric, Görtler vortices, Annu. Rev. Fluid Mech. **26**, 379 (1994).

[30] R. T. Davis and S. G. Rubin, Non-Navier Stokes viscous flow computations, Comput. Fluids **8**, 101 (1980).

[31] V. S. Pratap and D. B. Spalding, Numerical computations of the flow in curved ducts, Aeronaut. Q. **26**, 219 (1975).

[32] J. L. Guermond, P. Minev, and J. Shen, An overview of projection methods for incompressible flows, Comput. Methods Appl. Mech. Eng. **195**, 6011 (2006).

[33] O. Botella, On the solution of the Navier-Stokes equations using Chebyshev projection schemes with third-order accuracy in time, Comput. Fluids **26**, 107 (1997).

[34] D. Biau and A. Bottaro, An optimal path to transition in a duct, Philos. Trans. R. Soc. A **367**, 529 (2009).

[35] U. Ascher, S. Ruuth, and B. Wetton, Implicit-explicit methods for time-dependent partial differential equations, SIAM J. Numer. Anal. **32**, 797 (1995).

[36] R. W. MacCormack, The effect of viscosity in hypervelocity impact cratering, *4th Aerodynamic Testing Conference* (Cincinnati, Ohio, 2012).

[37] T. Watanabe and S. Yanase, Bifurcation study of three-dimensional solutions of the curved square-duct flow, J. Phys. Soc. Jpn. **82**, 074402 (2013).

[38] L. Wang and T. Yang, Periodic oscillation in curved duct flows, Physica D **200**, 296 (2005).

[39] L. S. Tuckerman, Computational challenges of nonlinear systems, *Emerging Frontiers in Nonlinear Science*, edited by P. G. Kevrekidis, J. Cuevas-Maraver, and A. Saxena (Springer International Publishing, Cham, 2020).

[40] S. Yanase, T. Watanabe, and T. Hyakutake, Traveling-wave solutions of the flow in a curved-square duct, Phys. Fluids **20**, 124101 (2008).

[41] P. A. J. Mees, K. Nandakumar, and J. H. Masliyah, Secondary instability of flow in a curved duct of square cross-section, J. Fluid Mech. **323**, 387 (1996).

[42] C. Castelain, A. Mokrani, Y. Le Guer, and H. Peerhossaini, Experimental study of chaotic advection regime in a twisted duct flow, Eur. J. Mech. B **20**, 205 (2001).

[43] H. Fellouah, C. Castelain, A. Ould El Moctar, and H. Peerhossaini, A criterion for detection of the onset of Dean instability in Newtonian fluids, Eur. J. Mech. B **25**, 505 (2006).

[44] J. Canton, E. Rinaldi, R. Örlü, and P. Schlatter, Critical Point for Bifurcation Cascades And Featureless Turbulence, Phys. Rev. Lett. **124**, 014501 (2020).

[45] J. Kühnen, P. Braunshier, M. Schwegel, H. C. Kuhlmann, and B. Hof, Subcritical versus supercritical transition to turbulence in curved pipes, J. Fluid Mech. **770**, R3 (2015).

[46] See Supplemental Material at http://link.aps.org/supplemental/10.1103/PhysRevFluids.6.024101 for the source code .